Holographic Temperature Measurement and Heat Flux Determination within the Thermal Boundary Layer

R.Müller and B.Ineichen

I.C. Engines and Combustion Technology Laboratory
Swiss Federal Institute of Technology
Sonneggstr.5, NOH 47, ETH-Zentrum, CH-8092 Zurich
Switzerland

ABSTRACT

Both theoretical and experimental problems associated with the quantitative evaluation of heat transfer through holographic interferometry and particle tracking are discussed. General considerations for heat transfer measurements are given and it is shown that in most cases temperature profiles can be determined from a single holographic interferogram. The experimental problem of fringe interpolation is solved with an opto-electronic phase measurement technique, which has a resolution of better than 1/1000 of a fringe spacing. The spatial resolution of the measurements was approximately 5-15 μm, and temperature profiles could be obtained at distances within 10 μm from the wall. The overall accuracy and reproducibility are theoretically and experimentally investigated.

To evaluate this technique for precise heat transfer measurements, the thermal boundary layer and the velocity field in front of a heated vertical test plate is discussed.

Numerical and theoretical investigations of heat transfer are envisaged including studies on e.g. the phonon heat conduction in solids and the effect of the deposition of a thin soot layer.

INTRODUCTION

In internal combustion engines heat and mass transfer play major roles. For engines, variables of interest include surface heat transfer, boundary layer temperature distribution and boundary layer thickness. In heat transfer experiments the objective among them is to determine the distribution of temperature throughout a gas or fluid. Because of heat transfer considerations the temperature profile of gases near walls is important. Moreover, the ability to accurately predict heat transfer using modeling would be an important tool for the design of efficient engine chambers (1, 2). The thermal boundary layer is in most cases a quantity estimated from engine thermodynamic calculations. Since the laminar sublayer thickness can be in the regime of micrometers, microscale heat transfer phenomena have to be considered. So far it is not possible to decide whether microscale heat transfer theory is applicable to engine heat transfer studies. The microscale approach relies on known physical foundations and the functional relation depends in e.g. scattering mechanism for phonon heat conduction.

There exist a wide range of potential techniques for measurements of temperature profile of gases near walls. Optical techniques are an attractive alternative to the use of intrusive probes, because they require only the passage of a low-intensity optical wave through the gas. Optical single point measurements have been applied to combustion problems by the use of Raman scattering, broadband coherent anti - Stokes Raman scattering (CARS) and others (3). Full-field temperature measurement methods include photography, interferometry, and techniques such as planar Raman scattering (4, 5).

In this paper we describe the use of heterodyne holographic interferometry for the quantitative determination of temperature profiles in boundary layers. This includes the development of a special opto-electronic system to increase the sensitivity and the accuracy for the interpolation of holographic interference patterns. In addition, a particle tracing method is described to determine the local velocity values.

BASIC CONSIDERATIONS

Heat transfer measurements in internal combustion engines are complex due to the non-steady pressure gradients, turbulence parameters and reaction zones. In steady-state conditions the physical mechanisms of heat transfer at the interface between the hot gas and the wall are basically the same as in dynamic considerations. Therefore, an appropriate test cell for steady-state vertical flow was envisaged. Classical theory for vertical flow with a vertically or horizontally located plate has been studied in great detail, in order that verification of the experimental results can be easily performed. Fig. 1 denotes the system variables and boundary conditions defining steady-state heat transfer. It envisages the difficulty in designing a test cell such as to reduce the experimental parameters as far as possible. In optimizing the experimental set up we ensure that the experimental data are those which are required for precise definition of heat transfer properties.

A test cell for experimental investigations of temperature profiles near the wall has to be designed so that

interactions with the environment can be neglected. Therefore, for later construction, some basic studies on the set up had to be discussed.

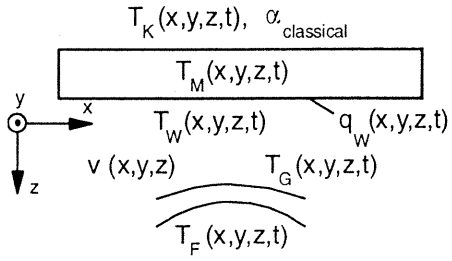

$T_G(x,y,z,t)$	temperature profile, incl. boundary layer
$q_W(x,y,z,t)$	source terms at the surface, i.e., oxidation
$T_M(x,y,z,t)$	heat conduction through the cross-section
$T_F(x,y,z,t)$	radiation partner flame, chamber walls
$T_K(x,y,z,t)$, $\alpha_{cl.}$	backside cooling
v (x,y,z,t)	velocity field

Fig. 1 General conditions defining steady-state heat transfer

Heat transfer due to convection and radiation can be simulated in finite element applications using well known models. Heat conduction is described by Fourier's law, where for the accuracy only temporal and spatial discretization are the limiting factors. In the finite element solver used in our study, temperature dependent properties are updated every time step during calculation. For boundary conditions, a set of Nusselt numbers is available for special convection configurations. Vertical flow is a well known situation, if only a qualitative heat transfer may be required. Radiation is considered as gray body radiation with a certain absorption and radiation ratio or temperature dependent spectra for the materials. Fig. 2 represents the schematic of a model including boundary conditions, involved to estimate heat transfer in a given experimental set up with vertical flow.

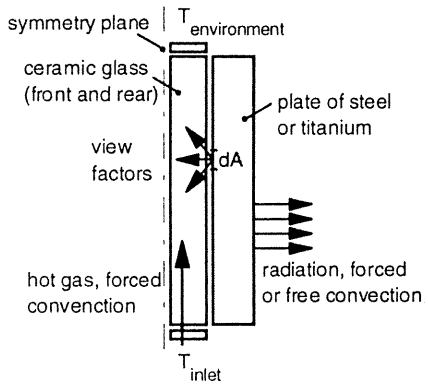

Fig. 2 Finite element model with boundary conditions for convection and radiation

The steady-state solutions for different boundary conditions, e.g. cooling of the plate by air or water and varying velocity and temperature for the convective heat transfer have been calculated for the test cell in these experiments. In conclusion, some of the heat transfer properties of Fig. 1 can be controlled by a closed, symmetrical cell with vertically oriented test plates of known geometry and that the flow of hot gas and cooling fluid has to be temperature and velocity controlled.

TEST CELL

Measurement of the temperature profile in the thermal boundary layer and the velocity of the hot gas are the main tasks of the experimental investigations on steady-state heat transfer.

A cross-section of the test cell that has been realized for heat transfer measurements, is shown in Fig. 3.

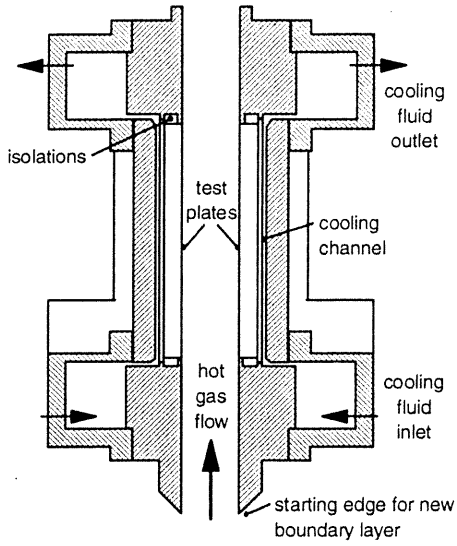

Fig. 3 Cross-section of the test cell

The plates are isolated along the edges to obtain a one-dimensional heat flux. Plates of different materials, i.e., steel or titanium with various surface roughness can be inserted to investigate the influences on heat transfer properties. An important condition is, that the boundary layer extends without influence of a thermal step. Identical materials are used to fulfill this condition.

The hot gas is produced by a flamelet burner below the test cell with adjustable flow rates. The propane flame is controlled by maximum air pressure of $1x10^5$ Pa and propane gas pressure of $0.5x10^5$ Pa. Any desired smaller flow rate is available by reduction valves. Thus, between the plates, a mostly laminar condition without any reaction zones can be generated.

TEMPERATURE MEASUREMENTS BY HETERODYNE HOLOGRAPHIC INTERFEROMETRY

There are methods to reconstruct three-dimensional phase objects from holographic interferometric data. The inverse scattering method (6) assumes that the intensity of the wave scattered by the object structure remains small compared with the intensity of the illuminating wave. In the case of realistic phase objects this is a very severe limitation,

and therefore experimental verification of the inverse scattering method has not yet been very successful. Furthermore, a set of observations with different directions of illumination must be used for complete reconstruction of the three-dimensional refractive index n(x, y, z).

Also in the straight-line approximation (7), a set of observations under different directions must be used for complete reconstruction of the three-dimensional refractive index n(x, y, z). This method requires that the average gradient of the refractive index is small enough so that the light paths through the object are straight lines within the considered spatial resolution. This condition is much less restrictive than the requirements for the inverse scattering method in phase objects. But still, in practical applications, serious problems occur in the numerical evaluation due to the non-regular distribution and the limited accuracy of the data samples obtained from the interferograms (8, 9).

With classical holographic interferometry (10, 11), determination of the interference phase is only reliable in the minima and maxima of the fringes. Each fringe represents a phase shift of 2π, thus maxima and minima appear at phase values $2N\pi$ and $(2N+1)\pi$. Along a fringe, temperature remains constant if pressure and material properties have not been changed significantly between the two exposures. Since interpolation between the fringes is an unknown non-linear function, determination of the phase field by classical holographic interferometry is bound to the coordinates of the fringes. Furthermore, in regimes of higher fringe concentration, background illumination and image noise due to the laser speckles reduce the fringe contrast. In investigations of heat transfer from a hot gas to a cooled wall this is a severe limitation according to the steep temperature gradients in the boundary layer near the wall.

In summary, there is still a strong need for a measurement technique in three-dimensions with higher resolution, lower noise and more accurate data acquisition.

Heterodyne holographic interferometry is a method that allows interpolation between the fringes at low noise and therefore gives access to much higher resolution.

Holographic Recording and Reconstruction

The basic idea of heterodyne holographic interferometry is to record two object fields with two reference waves on a hologram plate, such that the object fields are reconstructed independently. The introduction of a small frequency shift between the two reference waves results in an intensity modulation at the beat frequency for any given point in the interference pattern of the reconstructed light fields. The optical phase difference is converted into the phase of the beat frequency signals.

To envisage the differences compared with classical holographic interferometry, Fig. 4 shows a schematic of the set up required for the heterodyne method.

The object waves, O_1 and O_2, are stored independently with the two reference beams, R_1 and R_2. The angles between the references and object waves must be within the range given by the spatial frequency resolution of the holographic storage material. The spatial frequency f_y is geometrically defined by the angles of incidence onto the hologram of the reference and object light.

$$f_{y1} = \frac{\sin\theta_{R_1} + \sin\theta_{O_1}}{\lambda} \quad , \quad f_{y2} = \frac{\sin\theta_{R_2} + \sin\theta_{O_2}}{\lambda} \qquad (1)$$

The intensity ratios between object illumination and reference waves R_1 and R_2 can be adjusted independently by the two variable beam splitters S_1 and S_2 to get first optimum recording conditions and afterwards maximum power in the reconstructing reference waves.

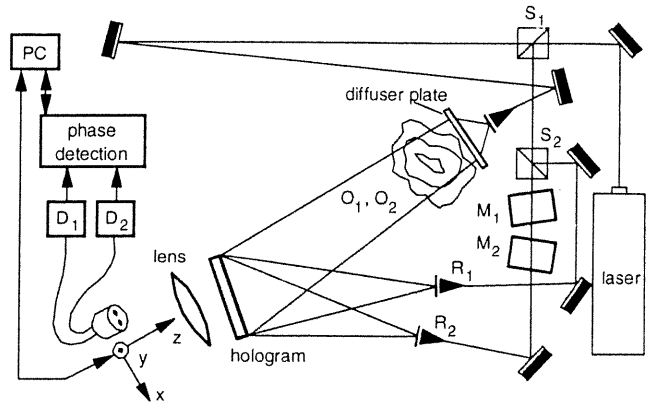

Fig. 4 Set up for heterodyne holographic interferometry: beam splitters S_1 and S_2, reference waves R_1 and R_2, object waves O_1 and O_2 and the two acousto-optical modulators M_1 and M_2; D_1 and D_2 are photodetectors

The use of two standard 40 MHz acousto-optical modulators in cascade is to produce zero frequency shift for the recording and 100 kHz for the reconstruction. Even with zero net shift frequency, recording has to be performed including the Bragg cells, because the angular set up for recording and reconstruction must be identical. The second modulator M_2 is mounted just behind the first one M_1, but rotated by 90° around the light beam. This is necessary to get all the possible combinations of diffracted beams completely separated in a plane at some distance from the two modulators. The first order diffractions are shifted in frequency by either $+\Omega$ or $-\Omega$, depending on whether the diffraction is in the direction of the traveling acoustic wave or opposite to it. The diffraction angles are typically 5 mrad, which is about 15 times the diffraction limited divergence of a 1 mm diameter laser beam. Switching from recording conditions to reconstruction conditions has negligible effects on the propagation of the diffracted beams, since the 100 kHz change of the 40 MHz acoustic wave changes the diffraction angle only by 0.01 mrad, which is smaller than the divergence of the laser beam.

In the reconstruction, the object is projected in a three-dimensional image behind the hologram where detectors, later to be discussed in detail, scan the phase field. Placed at a point (x, y, z = ∞) the photodetectors measure a sinusoidal signal independent of brightness variations of the background across the image. Superimposed with the Gaussian object illumination the local interference phase $\Delta\varphi$

between the two reconstructions is distributed on a periodic signal at the beat frequency $\Delta\Omega = \Omega_1 - \Omega_2$.

$$I(x,y,z) = |\Re_1 + \Re_2|^2 = a_1^2 + a_2^2 + 2a_1a_2\cos[\Omega t + \Delta\varphi(x,y,z)] \quad (2)$$

Because of the optical frequency shift, detection is inherently less sensitive to speckle noise than to fringe intensity modulations. A low limit for the value of the beat frequency is given by low frequency disturbances of the surroundings of the experimental set up and the corresponding percental fault in phase calculation. An upper limit is given by the edge frequency of the opto-electronic detectors. Thus, a difference frequency of 100 kHz is selected.

Phase Data Acquisition

The heterodyne method allows, in great advantage over classical holographic interferometry, free selection of grid point coordinates for scanning the phase field. At discrete depths along the viewing or, respectively, the illumination direction, detectors follow a mesh with selected Δx and Δy.

An appropriate photographic lens is placed behind the hologram to form an image of the object in the plane of observation. An array of two fiber bundles connected to photomultipliers is used to scan the image. The mostly sinusoidal signals of the two photomultipliers are analyzed by a digital signal oscilloscope and after Fast Fourier Transformation (FFT) the electronic phase difference of the two signals are determined. The detection array is mounted on a step motor driven stage to scan the image. The programmed scanning pattern is executed by the X-Y control unit. For any measured position the coordinates in the image plane as well as the electronic phases are stored on the computer, to be available for further data processing.

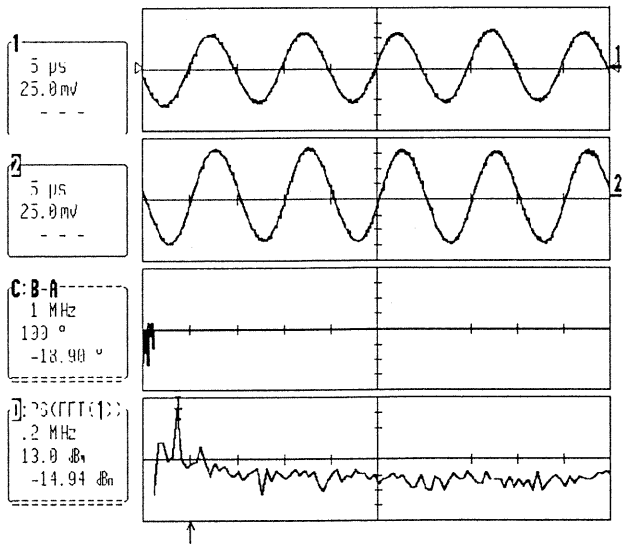

Fig. 5 Beat frequency signals envisaging the required analysis steps to obtain the phase difference from photodetector signals

The algorithm used for signal analysis is envisaged in Fig. 5. Phase spectrum calculation after FFT and cursor setting on the beat frequency of 100 kHz yielding the requested phase value.

While moving from one grid point to another, some phase values are obtained to detect locations of zero crossings. To reduce data, two regimes of different resolution can be selected. Only in the section of high fringe concentration near the wall, the detectors are moved in steps down to 10 µm, i.e., the resolution limit of the positioning system. The smallest detectable fringe distance is in the order of five times the fiber bundle diameter. Still, the overall phase difference between the object states can be adjusted to the desired resolution by selecting their mean temperatures for the exposures.

Temperature Determination

After reconstruction of the optical phase field, a temperature distribution is calculated.

For the scanning procedure, with z along the observation direction and Δz as the distance between the planes focused on various depths through the object, the optical path length difference between the two object states is a direct function of the refractive index variation.

$$\Delta\phi = \frac{\Delta\varphi(x,y,z)}{2\pi}\cdot\lambda = \sum_{z=0}^{z}(n-n_0)\cdot\Delta z \quad (3)$$

The Gladstone-Dayle equation describes the refractive index as a material dependent function of the system density.

$$n - 1 = K\cdot\rho \quad (4)$$

In combination with the ideal gas equation, the refractive index distribution is described as a function of the system variables, mostly temperature. Here, the material properties and pressure are assumed to be constant. In fact, this is a small restriction due to the dominant overall change in temperature.

$$n = K\cdot\rho(x,y,z) + 1 = \frac{KMp}{RT(x,y,z)} + 1 \quad (5)$$

A light beam probing a temperature and therefore refractive index gradient to the side, for example, the y coordinate, is slightly deflected and an additional phase difference has to be considered. According to (8), this results in a change of path length or refractive index. Since this sidewards deflection is evident in our application, this correction has to be considered in Eq. 3.

$$\Delta\phi = \sum_{z=0}^{z}\left(n(y_0) + \frac{1}{2}\cdot\frac{n'^2}{n(y_0)}\cdot z^2 - n_0\right)\cdot\Delta z \quad (6)$$

After initialization on a first focal plane or calculation in any further plane, the deflection and corresponding temperature difference have to be calculated for a corresponding point in the next plane. These informations

are available through the experimental data. The deflection is a function of the measured phase difference gradient between two neighboring points from one plane to another (Eq. 3). The corresponding temperatures are calculated through Eq. 5. Finally, the combination of Eq. 3 and Eq. 5 yield an optical phase change as a function of temperature which can be incrementally described throughout the object.

$$\Delta\varphi\Big|_{z_0}^{z_1} = \frac{KMp}{R}\cdot\left(\frac{1}{T(y_0)}-\frac{1}{T_0}+\frac{1}{2}\cdot\frac{\dfrac{KMp}{R(y-y_0)^2}\cdot\left(\dfrac{1}{T(y)}-\dfrac{1}{T(y_0)}\right)^2}{\dfrac{KMp}{RT(y_0)}+1}\cdot z^2\right)\cdot(z_1-z_0) \tag{7}$$

An iterative calculation of the local temperature T(y) starts with an assumption of a temperature at a point in the new focal plane compared with the corresponding point in the former plane z - Δz. The measured value on the left side of the equation should equal the calculated right side. The deflection y - y_0 can be obtained through the phase gradient between these points and is available through the phase values of the neighbor points. The procedure is repeated for every mesh point in the new focal plane and thus for further planes throughout the whole object, yielding the three-dimensional temperature distribution.

RESULTS, ACCURACY AND REPRODUCIBILITY

The overall accuracy and reproducibility of heterodyne holographic interferometry depend mainly on the signal-to-noise ratio (SNR) of the detector signals and the mechanical stability of the optical set up. The stability and accuracy of the phase measurement is electronically tested to be better than +/- 0.1° for clean input signals at 100 kHz. The phase measurement requires for proper operation a SNR of at least 20 dB and a noise bandwidth of less than the signal frequency. The noise introduces a phase error due to the fluctuations of the zero crossings. This means that a single measurement with SNR = 20 dB yields a phase error of 6°. This was reduced to 0.06° for an integration time of 100 ms and a frequency of 100 kHz.

The SNR was estimated of the detector signals from the holographic set up, the hologram efficiency, the laser power and the observed fringe contrast, which is equal to the depth of modulation of the detector output. The observed fringe contrast suffers from the unequal amplitudes of the two interfering light fields and any scattered or ambient light causes an additional background intensity and reduces therefore the depth of modulation. The SNR determined in our experiments was about 40 dB. Besides of the phase error due to amplitude noise, additional phase fluctuation may occur in the signal. These are mainly caused by optical instabilities, e.g. in the path length of the two reference waves, and by mechanical instabilities of the position of the detection array and reconstructed image. Both effects are reduced by averaging over the integration time of the phase measurement at a certain position. The overall accuracy of phase measurement, including these phase fluctuations, was determined experimentally. A double exposure, two reference beam hologram of an object was recorded. The phase difference between the signals, shown in Fig. 6, of the two detectors at a constant separation of 0.7 mm in the image plane indicated a typical phase measurement accuracy of +/- 0.3° with an integration time of 6 s. With shorter integration time, the measured phases showed statistical variations of 0.4° around the average value.

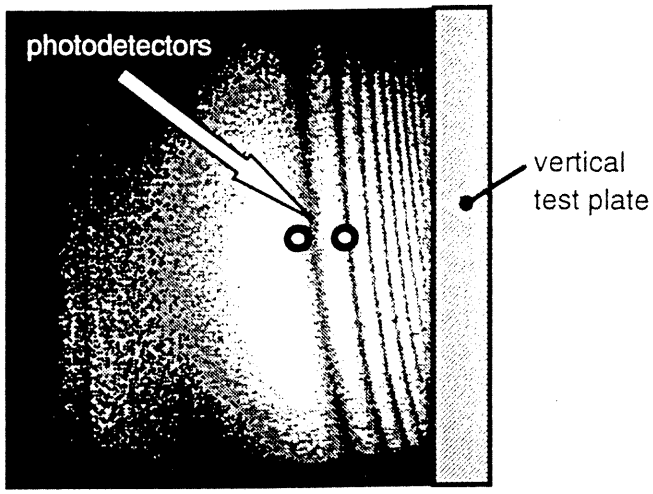

Fig. 6 Photodetectors positioned in a reconstructed double exposure hologram

The estimated absolute accuracy of the phase measurement is rather limited by the uncertainty of the mechanical and geometrical parameters, such as magnification factor, detector separation, than by the phase measurement itself. In summary, this corresponds to an interpolation accuracy better than 1/1000 of a fringe.

The hologram was recorded at 0.5 m distance from the test cell. The reconstruction was imaged with a magnification of 3.0 by a f/9 aperture objective (f = 400 mm), located closely behind the hologram. The detection array consists of two circular fiber bundles of 0.1 mm active diameter. The 2 mm separation of the two fiber bundles corresponds to a distance of 0.7 mm, and the fiber diameter of 0.03 mm in the object. The spatial resolution is determined by the translation stage in the image plane and has an overall accuracy of 10 um.

VELOCITY FIELD EVALUATION

For convection analysis, flow velocity is part of the boundary conditions. In a former paper (12), we discussed possibilities and restrictions of both, particle image velocimetry (PIV) and the speckle method.. In the same paper, a particle tracing method has been introduced. Added to the flow, the particles are illuminated by a laser sheet in a couple of pulses. This clearly identifies those particles remaining in the sheet during exposure and furthermore, the beginning and ending point of a trace is defined. After image analysis routines direction and magnitude of the velocity field can be determined.

CONCLUSIONS

It has been demonstrated, that for a successful determination of the temperature profile near the wall, it is necessary to use very accurate fringe interpolation. With an opto-electronic phase measurement technique, described in this paper, the required interpolation accuracy can be obtained. As demonstrated for the classical example of a heated plate the existing equipment has a resolution of better than 1/1000 of a fringe. The combination of hologram interferometry and high accuracy fringe interpolation has shown to be a powerful technique to collect data for quantitative reconstruction of three-dimensional refractive index distributions in transparent objects. The relation between the points of measurement in the image plane and the corresponding object points is obtained using the laws of geometrical optics. With the partial localization fringe method, temperature profiles in three-dimensional, asymmetric refractive index fields can be provided with a single hologram.

ACKNOWLEDGMENTS

The authors would like to express their appreciation to Prof. M. K. Eberle for his support in this investigation. They also wish to thank P. Eberli, S. Nguyen-Chi and A. Schmid for their contributions with the experiment. They are also indebted to P. Obrecht for skillful experimental assistance. Financial support was provided from the Swiss Commission for the Promotion of Scientific Research (KWF) Grant No. 2207.1.

NOMENCLATURE

a = real amplitude, J/m^2
f = spatial frequency, mm^{-1}
I = intensity, J/m^2
K = Gladstone-Dayle constant, m^3/kg
M = molecular weight, -
N = fringe order number, -
n = refractive index, -
p = pressure, Pa
R = universal gas constant, 8.3143 J/mol K
$\Re$ = reconstructed complex amplitude, $J^{-0.5}/m$
T = temperature, K
t = time, s
φ = optical phase, deg
ϕ = optical pathlength, m
λ = optical wavelength, m
θ = angle of incidence, deg
ρ = density, kg/m^3
Ω = acoustic frequency, s^{-1}

Subscripts
R = reference light
O = object light
y = horizontal and perpendicular to the hologram plate

REFERENCES

1. Diwakar, R., "Assessment of the Ability of a Multidimensional Computer Code to Model Combustion in a Homogeneous-Charge Engine," SAE Paper No. 840230, SAE Trans. Vol. 93, pp. 2.85-2.108, 1984.

2. Ikegami, M., Kidoguchi, Y. and Nishiwaki, K., "A Multidimensional Model Prediction of Heat Transfer in Non-Fired Engines," Int. J. Heat Mass Transfer Vol. 27, pp. 1873-1878, 1984.

3. Penner, S. S., Wang, C. P., and Bahadori, M. Y., "Laser Diagnostics Applied to Combustion Systems," Twentieth Symposium on Combustion, p. 1149, 1985.

4. Long, M. B., Levin, P. S. and Fourguette, D. C., "Simultaneous Two-Dimensional Mapping of Species Concentration and Temperature in Turbulent Flames," Opt. Letters Vol. 10, p. 267, 1985.

5. Vest, C. M., "Holographic Interferometry," J. Wiley & Sons, New York, pp. 315-334 / 363-373, 1979.

6. Carter, W. M., "Computational Reconstruction of Scattered Objects from Holograms," J. Opt. Soc. Am. Vol. 60, pp. 306-314, 1970.

7. Rowley, P. D., "Quantitative Interpretation of Three-Dimensional Weakly Refractive Objects Using Holographic Interferometry," J. Opt. Soc. Am. Vol 59, pp. 1496-1498, 1969.

8. Sweeney, D. W. and Vest, C. M, "Reconstruction of Three-Dimensional Refractive Index Fields from Multidirectional Interferometric Data," Appl. Optics Vol. 12, pp. 2649-2664, 1973.

9. Vest, C. M. and Radulovic, P. T., "Measurement of Three-Dimensional Temperature Fields by Holographic Interferometry," Applications of Holography and Optical Data Processing, Pergamon Press, Oxford, pp. 241-249, 1977.

10. Dändliker, R. and Weiss, K., "Reconstruction of the Three-Dimensional Refractive Index from Scattered Waves," Opt. Commun. Vol. 1, pp. 323-328, 1970.

11. Wolf, E., "Determination of the Amplitude and the Phase of Scattered Fields by Holography," J. Opt. Soc. Am. Vol. 60, pp. 18-20, 1970.

12. Ineichen, B. and Müller, R., "Development of Laser Diagnostic Techniques for Full-Field Velocity Measurements," Proceedings of Third International Symposium Topics in Chemical Propulsion: Non-Intrusive Combustion Diagnostics, Scheveningen / Netherlands, 1993.